Nuclear Instruments and Methods in Physics Research B 494-495 (2021) 46–52

Contents lists available at ScienceDirect

Nuclear Inst. and Methods in Physics Research, B

journal homepage: www.elsevier.com/locate/nimb

Influence of beam power on the surface architecture and corrosion behavior of electron-beam treated Co-Cr-Mo alloys

S. Valkov [a], S. Parshorov [b], A. Andreeva [c], S. Rabadzhiyska [a], M. Nikolova [d], R. Bezdushnyi [c], P. Petrov [a]

[a] Institute of Electronics, Bulgarian Academy of Sciences, 72 Tsarigradsko Chaussee blvd., 1784 Sofia, Bulgaria
[b] Institute of Metal Science, Equipment and Technologies with Hydro- and Aerodynamics Centre, Bulgarian Academy of Sciences, 67, Shipchenski Prohod Blvd, 1574 Sofia, Bulgaria
[c] Faculty of Physics, St. Kliment Ohridski University of Sofia, 5 James Bourchier Blvd, 1164 Sofia, Bulgaria
[d] Department of Material Science and Technology, University of Ruse, 8 Studentska Str., 7017 Ruse, Bulgaria

ARTICLE INFO

Keywords:
Co-Cr-Mo alloys
Electron-beam surface treatment
Surface topography
Corrosion resistance

ABSTRACT

We present results of the influence of the electron beam power on the structure, surface roughness, and corrosion of electron-beam surface-treated Co-Cr-Mo alloys. The structure of the samples is characterized using X-ray diffraction (XRD), Scanning Electron Microscopy (SEM), and energy-dispersive X-ray spectroscopy (EDX). Atomic force microscopy (AFM) is used for the evaluation of the surface topography. The corrosion resistance is studied by an electrochemical test. The EBST process leads to a transformation in the phase composition, from a double-phase structure of ε and γ to a single-phase gamma structure. Higher values of the beam power lead to the elimination of pores and other structural defects, as well as a formation of preferred crystallographic orientation. The EBST causes a slight increase in the surface roughness and significantly more symmetrical surface topography. Also, the corrosion resistance was greatly improved after electron-beam surface treatment with higher values of the electron beam power.

1. Introduction

The Co-Cr-Mo alloys have many biomedical applications and are considered as a joint replacement due to their biocompatibility and attractive mechanical properties [1–5]. However, the biological corrosion could lead to a separation of metallic ions which results in disadvantageous reactions and implant failure [6]. The discussed limitations depend mostly on the properties on the surface and can be improved by an appropriate technique for surface modification. The authors of [7] have demonstrated that the corrosion resistance of Co-Cr-Mo alloys was greatly improved after carbon ion implantation. Lutz et al. [8] have investigated the tribocorrosion of medical Co-Cr-Mo alloy after nitrogen insertion and concluded that the properties depend on the temperature of the process. Their results showed that low temperatures led to greater corrosion resistance and better tribological properties .

In recent years, high energy fluxes (e.g. laser or electron beams) are frequently used for the manufacturing and the improvement of the surface properties of the materials. These technologies are characterized by very high thermal cycle gradients, leading to structural changes [9]. Wei et al. [10] have optimized the technological conditions of surface modification of Co-Cr-Mo by laser interference lithography and the results showed the hardness and tribological properties were significantly enhanced. The authors of [11] have discussed the influence of the mechanism of formation on the structure and properties of Co-Cr-Mo alloys fabricated by selective laser melting (SLM) and the results were compared with ASTM F75 standard (a non-magnetic Co-Cr-Mo alloy with high strength, corrosion resistance, and excellent wear resistance). It was demonstrated that the tensile strength, yield strength, and hardness of SLM manufactured material exceed that of the ASTM F75 standard [11].

Currently, electron-beam technologies receive a lot of attention due to the possibility of precise control of the technological conditions. These methods are among the most promising for manufacturing and surface modification due to the uniform distribution of the energy, very short process time, reproducibility, etc. [12–20]. Sun et al. [21] have studied the influence of the microstructure inhomogeneity on the creep behavior of Co-Cr-Mo alloy built-up by electron beam melting. The results showed that the phase composition of the material changes from stable ε-hcp at the earlier stages of growth to metastable γ-fcc Co at more advanced levels. The ε-grains were larger at the initial points (i.e. the bottom of the specimen) in comparison with those from the upper parts. It was concluded that the grain size significantly affects the creep resistance. The authors of [22] have studied the manufacturing of Co-Cr-Mo implants with the addition of 0.04% Zr by electron beam melting.

https://doi.org/10.1016/j.nimb.2021.03.007
Received 15 February 2021; Accepted 8 March 2021
Available online 20 March 2021

Table 1
Chemical composition of the specimens treated by an electron beam power of 500 W and 750 W.

Sample	Co, wt%	Cr, wt%	Fe, wt %	Mo, wt%	Other elements, wt%
500 W	60.2	27.4	4.5	7.1	0.2
750 W	65.9	23.9	5.1	4.6	0.5

Their results showed that bone tissue is in direct contact with the implant materials and the low amount of Zr further improves the anchorage of the bone to the alloy. It was concluded that electron beam melting technology is an appropriate one for implant manufacturing. Tan et al. [23] have studied the precipitation characteristics of carbides in Co-Cr-Mo parts manufactured by electron beam melting. It was shown that a lot of carbides have precipitated within the interdendritic regions and at the grain boundaries.

Our previous investigations [24] were based on electron-beam surface treatment (EBST) of conventionally manufactured Co-Cr-Mo alloys, where a transformational treatment (i.e. without the formation of a melt pool [25]) was applied. The results of [24] showed that the surface roughness was increased and the corrosion properties were enhanced after the EBST. The authors of [25] have analyzed the transformational (i.e. without the formation of a melt pool) and melting (i.e. with the formation of a melt pool) approaches of electron-beam surface treatment and concluded that the materials subjected to melting exhibit better functional properties due to the increase in the hardness and favorable distribution of the stresses. Although the application of the melting treatment leads to better functional properties in comparison with the transitional treatment, the EBST of Co-Cr-Mo alloys by melting the treated surface and formation of a melt pool (melting treatment) is less well investigated.

This study aims to investigate the effect of electron-beam surface treatment via a melting approach of as-casted Co-Cr-Mo alloy on the surface architecture and corrosion behavior.

2. Experimental part

Ingots of Co-Cr-Mo based alloy with a chemical composition of 25.5%-Cr, 0.2%-Mn, 4.3%-Fe, 59.9%-Co, 1.0%-Ni, 4.7%-Mo, 0.6%-W, 3.8%-other elements, in wt%, were manufactured by cast method and samples with dimensions of 20 × 20 × 4 mm were cut out by electro-erosion cutting method. The specimens were electron beam surface-treated where a scanning continuous electron beam was used. During the experiments, the accelerating voltage was 50 kV, the electron beam scanning frequency was 1 kHz; the velocity of the sample movement was 5 mm/sec. The electron beam current was 10 mA and 15 mA, corresponding to a beam power of 500 W and 750 W, respectively. The experiments were done using linear trajectory. With this manner of scanning, the thermal cycle gradient is the highest because the trajectory of the electron beam does not overlap (Fig. 1).

The phase composition and the formation of preferred crystallographic orientation of the specimens were studied by X-ray diffraction (XRD) using CuKα (1.54 Å) radiation. The measurements were performed in symmetrical mode from 35° to 80° with a step of 0.1° and a counting time of 10 sec per step.

The structure of the samples was investigated by scanning electron microscopy LYRA XMU (Tescan), equipped with an EDX detector (Quantax 200, Brucker). During the experiments, back-scattered electrons were used.

The surface architecture and roughness of the samples were investigated by Atomic Force Microscopy (AFM) using non-contact mode. During the experiments, a silicon tip with a radius of 10 nm was used. The scanned areas were chosen to be 20 × 20 μm along the x and y-axis, respectively. The number of measured heights along x and y directions was 512.

The corrosion resistance was studied in 80 ml naturally aerated

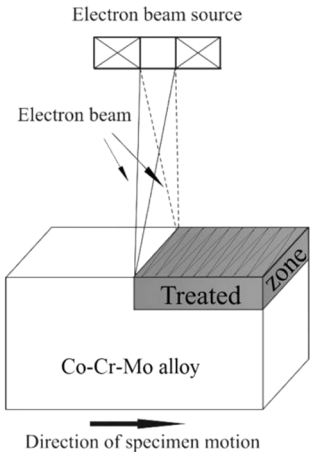

Fig. 1. Scheme of electron-beam surface treatment procedure.

artificial saliva (Fusayama) solution containing KCl (0.4 g/l), NaCl (0.4 g/l), $CaCl_2{\cdot}2H_2O$ (0.795 g/l), $NaH_2PO_4{\cdot}2H_2O$ (0.690 g/l), $Na_2S{\cdot}9H_2O$ (0.005 g/l), CH_4N_2O (1 g/l) with pH 5 (decreased with 1 N HCl) at room temperature. The potentiodynamic polarization curves were recorded by sweeping the potential starting at a cathodic potential about 250 mV below the OPC up to +2000 mV vs. Ag/AgCl at a scan rate of 1 mV s^{-1}. Tafel extrapolation method was used for obtaining the corrosion potential (Ecorr) and the density of the corrosion current (Icorr). The Stern-Geary equation was used for the determination of the polarization resistance (Rp).

3. Results and discussion

The experimentally obtained XRD patterns of the untreated and electron beam treated Co-Cr-Mo alloys are shown in Fig. 2. All diffraction maxima are indexed according to the ICDD crystallographic database, PDF # 05-0727 for ε-Co, and PDF # 15-0806 for γ-Co. The initial Co-Cr-Mo alloy (untreated) exhibits a biphasic structure of ε and γ phases. The ε phase is characterized by a hexagonal closed-packed (hcp) crystal structure and is thermodynamically stable at room temperature, while γ has a face-centered cubic (fcc) structure and is known as a high-temperature modification. The transformation from ε-Co to γ-Co occurs at about 900 °C, meaning that during the manufacturing of the ingots of Co-Cr-Mo based alloy, the phase composition was in the form of γ phase. After the subsequent cooling down to room temperature, the alloy becomes in the form of ε. However, the phase transformation from γ to ε

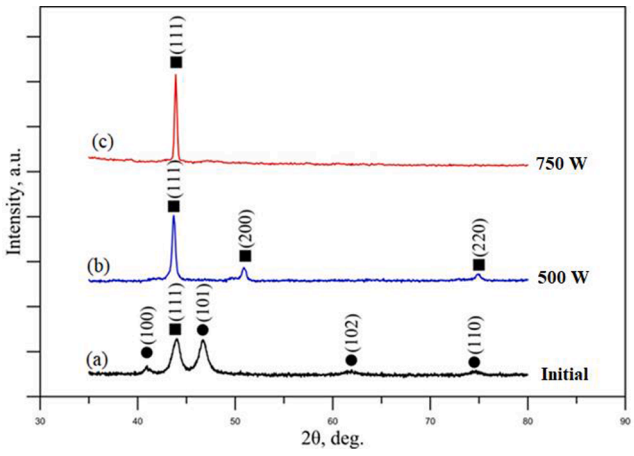

Fig. 2. X-ray diffraction patterns of Co-Cr-Mo alloy (a) initial specimen; (b) electron-beam treated with a beam power of 500 W; (c) electron-beam treated with a beam power 750 W.

occurs very sluggishly and a small amount of fcc phase, which is metastable at room temperature exists [26,27]. This is consistent with the XRD results pointing to a double phase structure, where the main one is ε, with some traces of γ phase. Considering the XRD patterns of the electron-beam treated specimens, it is evident that both samples exhibit a single-phase structure of gamma. As already mentioned, the electron-beam surface treatment process is characterized by a very high cooling rate (about 10^5 K/s for continuous mode) [16]. Also, during the EBST, the temperature of the treated zone of the material significantly exceeds 900 °C, meaning that the phase composition was in the form of γ, which is stable at high temperatures. As already mentioned, the transformation from fcc to hcp (i.e. from γ to ε) is too sluggish, and does not occur at the subsequent rapid cooling after the EBST process. These statements are consistent with the studied phase composition, showing that the EBST of the Co-Cr-Mo specimens leads to a transformation from a double phase ε and γ to γ structure. Considering the XRD patterns of both electron-beam surface-treated specimens, it is evident that the sample treated with a beam power of 500 W has a polycrystalline structure, where the XRD pattern exhibits diffraction peaks related to (111), (200), and (220) planes, while the diffractogram of the other (i.e. treated with a beam power of 750 W) exhibits only a diffraction maximum of (111). This means that the rise in the beam power leads to a reorientation in the micro-volumes of the Co-Cr-Mo alloys. The EBST process is characterized by a very high thermal cycle gradient, resulting in a formation of thermal stresses, and could have activated deformation mechanisms. This leads to a change in the orientation in the micro-volumes and the formation of a preferred crystallographic orientation [28,29].

A scanning electron microscopy (SEM) image of the untreated Co-Cr-Mo alloy is presented in Fig. 3. The results reveal a biphasic structure of ε and γ. The obtained results from the SEM analysis are consistent with those from XRD. Also, some pores can be seen, meaning that the structure of the untreated Co-Cr-Mo alloy is porous. This is a normal feature for the alloys prepared by casting methods due to the evolution of gases dissolved within the liquid material [30]. A cross-sectional SEM micrograph of the electron-beam treated with a beam power of 500 W specimen is presented in Fig. 4(a). A distinguished 5 μm thick re-melted zone (indicated as zone A) was formed, and the base material is marked as B. The structure of the re-melted layer is in the form of a single-phase structure, and no traces of the second phase can be observed. These results are consistent with those from XRD, confirming the existence of a single-phase structure of gamma after EBST with a beam power of 500 W. Also, the pores were eliminated, but some other structural defects and imperfections still exist. During the electron-beam surface treatment process, a large high-temperature gradient within the melt pool occurs, which causes an intense Marangoni convection. This convection is responsible for the homogenization, elimination of pores and other defects, etc. [31]. However, the lifetime of the melt pool is too short, and the input energy density is low, corresponding to lower surface temperature. In this case, the convection is not sufficient for melt homogenization, and some structural defects still remain.

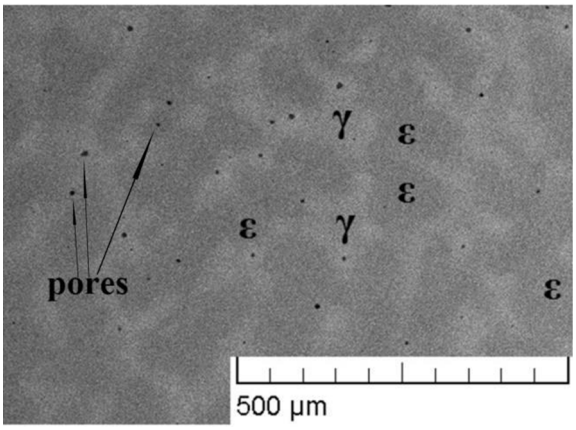

Fig. 3. A SEM micrograph of the untreated Co-Cr-Mo specimen.

A cross-sectional SEM micrograph of the specimen treated with an electron beam power of 750 W is shown in Fig. 5. The re-melted layer is marked as zone A, and its thickness is about 70 μm. The base material is indicated as zone B. Compared to the previous case (i.e. EBST with a beam power of 500 W), the EBST of the Co-Cr-Mo alloy with a beam power of 750 W leads to the formation of a re-melted layer with significantly higher thickness, which is attributed to the significantly higher beam power and input energy density [32], leading to a higher penetration depth of the electrons. The re-melted layer is in the form of a single-phase structure, which is again consistent with results from XRD measurements. No pores and other defects can be seen, and the quality of the re-melted layer was significantly improved in comparison with the case of e-beam treatment with a beam power of 500 W. As already mentioned, with an increase in the beam power the Marangoni convection is intensified, leading to a reduction of the pores and other defects [31]. The chemical compositions of the re-melted layers of both electron-beam treated samples were studied by energy-dispersive X-ray spectroscopy (EDX). The experimentally obtained spectra are shown in Figs. 4(b) and 5(b). The results are summarized in Table 1. No significant change (i.e. no more than 5 wt%) can be observed, meaning that the treatment process using the above-mentioned technological conditions does not affect significantly the chemical composition.

Fig. 6 presents the three-dimensional surface architecture of the initial Co-Cr-Mo alloy (Fig. 6(a)), and the electron-beam treated specimens with a beam power of 500 W (Fig. 6(b)), and 750 W (Fig. 5(c)). The considered micrographs are different, meaning that the electron-beam surface treatment process can significantly affect the surface topography. It is obvious that on the top of the initial sample, some surface formations (i.e. peaks and valleys) with different heights and depths are randomly distributed on the investigated area. This means that although the initial specimen was mechanically wet ground with grinding papers of 320, 400, 600, 800, and 1000, residual roughness exists. Considering the specimen treated with a beam power of 500 W, the randomly distributed peaks and valleys were replaced by a wave-like surface architecture. During the EBST process, the peaks are melted and the material flows to the valleys, forming a relatively flat surface. Meanwhile, fluid flows, formed due to the high-temperature gradient, act in the melt pool, and are responsible for the formation of the wave-like surface topography of the sample processed with a beam power of 500 W.

As the beam power rises to 750 W (Fig. 6(c)), it is evident that the surface architecture is in the form of homogeneously distributed peaks with relatively equal heights. During the EBST with a beam power of 750 W, the process can be associated with evaporation of the Co-Cr-Mo material. The subsequent condensation of the vapors should result in the formation of the observed peaks-like formations on the top of the specimen [33].

For a better understanding of the influence of the EBST technique on the surface roughness of the studied specimens, it was quantitatively expressed by the mean roughness S_a parameter, according to Eq. (1):

$$S_a = \frac{1}{M^*N}\sum_{k=0}^{M-1}\sum_{l=0}^{N-1}|z(x_k, y_l) - \mu| \quad (1)$$

Here, M and N represent the number of measured heights along the x and y directions, z is the measured height; x_k and y_l are the coordinates of a measured point. In (1) μ is the average height of the investigated area. Higher values of S_a correspond to higher surface roughness. Additionally, the distribution of the measured heights was evaluated by the S_{sk} parameter, which is a characteristic of the distribution of the heights symmetry/asymmetry, and it is given by (2):

$$S_{sk} = \frac{1}{(M^*N)^*\sigma^3}\sum_{k=0}^{M-1}\sum_{l=0}^{N-1}[z(x_k, y_l) - \mu]^3 \quad (2)$$

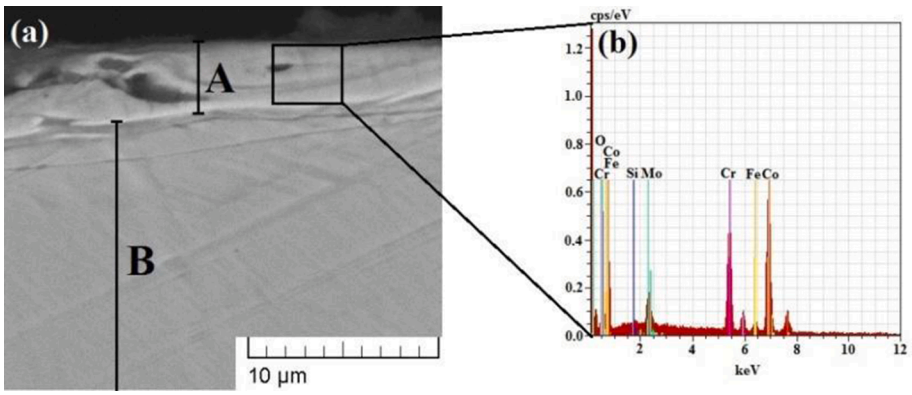

Fig. 4. (a) A cross-sectional SEM micrograph of the Co-Cr-Mo specimen treated with an electron beam power of 500 W; (b) corresponding EDX spectrum of the electron-beam treated area.

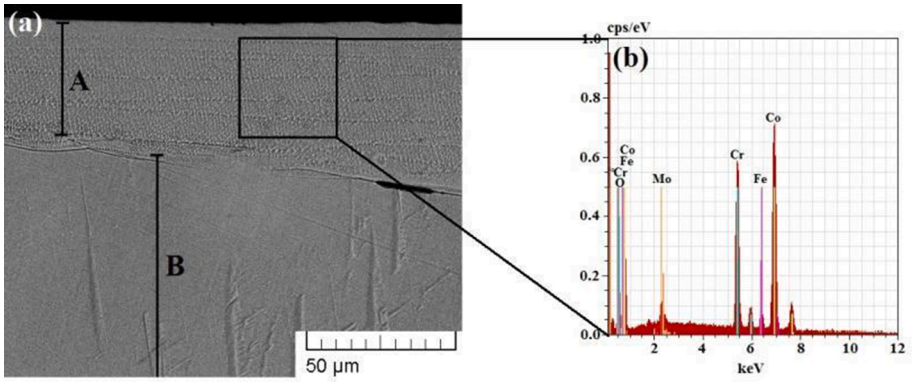

Fig. 5. (a) A cross-sectional SEM image of the Co-Cr-Mo specimen treated with an electron beam power of 750 W; (b) corresponding EDX spectrum of the electron-beam treated area.

Table 2
Statistical parameters of the surface roughness and corrosion properties of the untreated and treated with a beam power of 500 W and 750 W Co-Cr-Mo alloys.

Sample	S_a,nm	S_{sk}	E_{corr},mV	j_{corr}, μA/cm^2	R_p,MΩms
Untreated	19.17	0.84	−294	0.124	1.6
500 W	24.77	0.08	−216	0.150	1.5
750 W	20.51	0.13	+132	0.020	11

In (2), σ is the standard mean square deviation and can be written as follows:

$$\sigma = \sqrt{\frac{1}{(M^*N)-1}\sum_{k=0}^{M-1}\sum_{l=0}^{N-1}[z(x_k,y_l)-\mu]^2} \quad (3)$$

The parameter S_{sk} is a measure of the symmetry/asymmetry of the heights distribution, where the closer the value to zero, the more symmetrical distribution. If S_{sk} is equal to zero, the distribution of the heights is completely symmetrical. In the case of positive S_{sk} , the heights of peaks are larger than the depths of valleys, and vice versa.

The results for S_a and S_{sk} are summarized in Table 2. Considering the surface roughness of the investigated samples, a small increase in S_a can be seen after the electron-beam surface treatment process, meaning the surface of the EBST specimens is a bit rougher in comparison with the untreated one. According to Ref. [34], the electron-beam surface treatment process has a different influence in the case of rough and polished surfaces. Considering the samples, where the roughness is significant, the EBST can play the role of a polishing method due to the melting of the peaks, and the melted material flows and fills the valleys. For flat surfaces, the treatment process can lead to an increase in the surface roughness due to the formation of craters, as well as convection flows, which act in the melt pool. In the present particular case, the specimens were mechanically wet ground with grinding papers of 320, 400, 600,

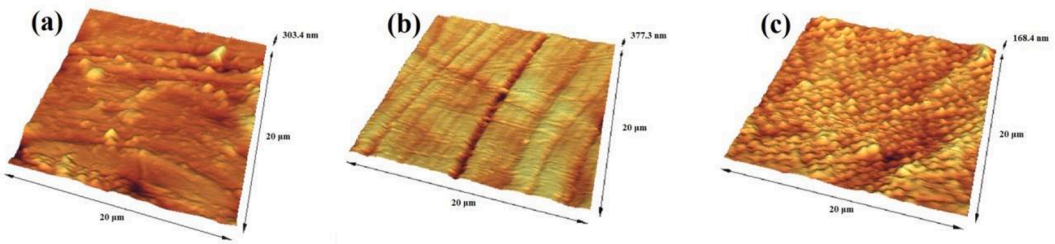

Fig. 6. Three dimensional AFM micrographs of the surface architecture of the specimens: (a) initial; (b) treated with a beam power of 500 W; (c) treated with a beam power of 750 W.

800, and 1000, but residual roughness still exists, meaning that a significant increase in this surface parameter could not be expected. However, the calculated values for the S_a parameter show that the roughness of the EBST samples is a bit higher than the untreated ones. Considering the symmetry/asymmetry of the heights distribution, it is evident that the application of the EBST leads to significantly closer values of S_{sk} to zero and much more symmetry of the distribution of the peaks and valleys. Also, in all cases, the values of S_{sk} are positive, pointing to higher heights than the depths of the valleys.

From a practical point of view, these results could have some advantages related to quick and lasting osseointegration. The biological advantage of periodic surface structures that reproduce the texture of the bone matrix is known to be the enhancement of osteogenic cell activity to form new bone [35]. Additionally, Çelen S. et al. found that the mesoscale 3D topography has the advantage of minimizing the stress shield between the implant and bone [36]. Also, the clinical advantage of the periodic textured surfaces might be related to the capacity of these surfaces to create micromechanical anchorage with the bone that turns out to be a stronger graft fixation than for machined surfaces [37].

The corrosion resistance of the considered samples was studied by an electrochemical experiment in 3.5 wt% NaCl solution at room temperature. The experimentally obtained polarization curves of the untreated and electron-beam surface-treated Co-Cr-Mo alloys are shown in Fig. 7, and the corrosion parameters are summarized in Table 2. Considering the corrosion current density (j_{corr}), the values related to the initial sample, and the treated one with a beam power of 500 W, are similar. However, the specimen treated with a beam power of 750 W exhibits a decrease in the j_{corr} by an order of magnitude, meaning that the corrosion rate is significantly lower in comparison with the initial and EBST with 500 W ones [38,39]. Also, both electron-beam treated specimens exhibit higher values of corrosion potential (E_{corr}), wherein in the case of treatment with a beam power 750 W, the discussed increase is significant. Lower values of the corrosion potential correspond to less susceptibility to corrosion [38,39]. Therefore, the experimental results for the corrosion resistance of the untreated and EBST Co-Cr-Mo alloys clarified that the EBST process leads to an improvement in the corrosion properties, especially in the case of treatment with a beam power of 750 W.

The improvement of the corrosion properties of electron-beam surface processed materials is attributed to the cleaning effect from undesirable inclusions, the formation of a re-melted layer which is much more homogeneous than the substrate, and reduction or even complete removal of pores and other structural defects [40–42]. As mentioned above, the structure of the initial (untreated) Co-Cr-Mo specimen is porous. The electron-beam surface treatment with a beam power of 500 W eliminates the pores, but some structural imperfections still exist. For this reason, the corrosion resistance of the specimen has not been significantly improved. As the beam power rises to 750 W, the structure of the re-melted layer has been significantly improved, and no or very few pores and other structural defects exist. This improvement in the structure of the re-melted layer of the sample treated with a beam power of 750 W is completely consistent with the enhancement in the corrosion properties.

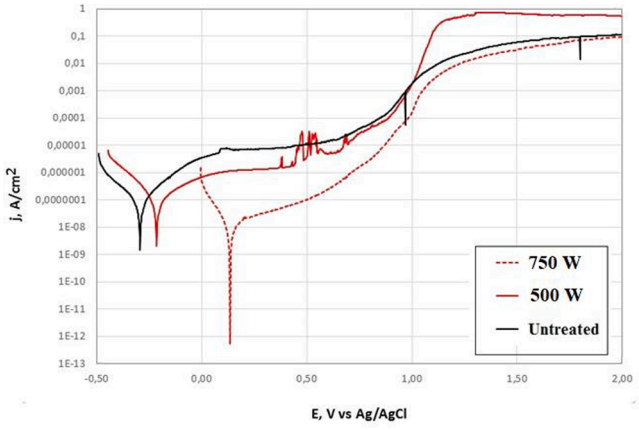

Fig. 7. Polarization curves of the untreated and electron-beam surface treated with a beam power 500 W and 750 W Co-Cr-Mo alloys.

This improvement can be attributed also to the crystallographic orientation [43–45]. The role of the texture in the corrosion properties is of major importance. In the case of orientation to the densely packed planes, the dissolution of the material occurs significantly slower in comparison with the loosely packed surface due to the lower surface energy. Materials that have a crystallographic texture towards the highly-dense plane are characterized by low surface energy and are expected to exhibit significantly better corrosion properties. This is again consistent with our results. As mentioned above, the EBST process with a beam power of 750 W led to a reorientation in the micro-volumes towards the densest plane (1 1 1), which exhibits the best corrosion resistance.

This study presents results of the electron-beam treatment and modification of the surface structure and properties of Co-Cr-Mo alloys. Before the treatment process of the Co-Cr-Mo material, the main phase was ε with a small amount of γ. The application of the EBST led to a transformation from the discussed bi-modal to a single-phase fcc-γ structure was observed. This could have some benefits from a practical point of view. The crystallographic structure has a significant influence on the functional characteristics of the materials. For example, the plasticity and the toughness are the highest in cases when the number of the slip systems is the highest. The plastic deformation is realized by movement of dislocations, as the main mechanism is the slipping, carried out in certain slipping systems, defined by a crystallographic plane and a crystallographic direction lying in it. The planes, in which the slip takes place, called the planes of slip, depend on the crystallographic structure and correspond to the most densely packed planes of the material. The sliding directions are the most tightly packed strands located in them [46,47]. It is known that the number of slip systems in cubic structures is higher than the hexagonal lattices, corresponding to better functional properties. Therefore, the Co-Cr-Mo alloy with a phase composition of a single fcc structure (i.e. gamma phase) should be characterized with much better functional properties. As already mentioned, the observed phase transformation, from the hexagonal closed-packed to a face-centered cubic structure after the EBST is attributed to the very high cooling rate at the treatment process [16]. Therefore, the cooling rate is very important for the structural changes of Co-Cr-Mo material. Moreover, the EBST technology is very promising for controlling the cooling rate due to the possibility for the realization of different scanning geometries [48]. For example, it is known that the application of a linear manner of scanning (Fig. 1) leads to a significantly higher cooling rate than the circular one because of the beam trajectory overlap at the latter approach. Therefore, the resultant structure and properties of the treated materials can be precisely controlled. This advantage of the EBST technology leads to the possibility of control of the functional properties of the treated material, which is one of the major advantages in comparison with the other methods for structure and properties modification.

4. Conclusion

In this study, we present results on the modification of Co-Cr-Mo alloys by electron-beam surface treatment (EBST) technique. The influence of the electron beam power on the structure, surface roughness, and corrosion of the material was investigated.

The results show that the EBST process leads to a transformation in the phase composition, from a double-phase structure of ε and γ to a single-phase gamma structure. As the beam power rises, from 500 W to 750 W, a formation of preferred crystallographic orientation towards the

(1 1 1) plane is observed. Higher values of the beam power leadto the elimination of pores and other structural defects. The EBST process causes a slight increase in the surface roughness and significantly more symmetrical surface topography. Also, the corrosion resistance is greatly improved after electron-beam surface treatment with a beam power of 750 W.

The main advantage of the EBST technology, as compared with the traditional methods for modification of the structure and properties, is the possibility to control the thermal cycle gradients during the process. This allows control of the resultant functional characteristics of the obtained re-melted layer, which, in turn, could open new potential applications of the EBST materials in industry.

CRediT authorship contribution statement

S. Valkov: Methodology, Conceptualization, Formal analysis, Writing - original draft. **S. Parshorov:** Methodology, Conceptualization. **A. Andreeva:** . **S. Rabadzhiyska:** . **M. Nikolova:** Writing - review & editing. **R. Bezdushnyi:** . **P. Petrov:** Supervision, Funding acquisition, Writing - review & editing.

Declaration of Competing Interest

The authors declare that they have no known competing financial interests or personal relationships that could have appeared to influence the work reported in this paper.

Acknowledgement

The financial support from the Bulgarian National Science Fund, project No. DN 17/17 is highly appreciated.

References

[1] Y.S. Al Jabbari, Physico-mechanical properties and prosthodontic applications of Co-Cr dental alloys: A review of the literature, J. Adv. Prosthodont. 6 (2014) 138.
[2] P.-A. Vendittoli, T. Amzica, A.G. Roy, D. Lusignan, J. Girard, M. Lavigne, Metal ion release with large-diameter metal-on-metal hip arthroplasty, J. Arthroplasty 26 (2011) 282–288.
[3] M. Niinomi, Recent metallic materials for biomedical applications, Metall. Mater. Trans. A 33 (2002) 477–486.
[4] J. Li, H. Ren, C. Liu, S. Shang, The effect of specific energy density on microstructure and corrosion resistance of CoCrMo alloy fabricated by laser metal deposition, Materials 12 (2019) 1321.
[5] G. Allegri, A. Colpani, P. Ginestra, A. Attanasio, An experimental study on micro-milling of a medical grade Co-Cr-Mo alloy produced by selective laser melting, Materials 12 (2019) 2208.
[6] Y. Abu-Amer, I. Darwech, J.C. Clohisy, Aseptic loosening of total joint replacements: mechanisms underlying osteolysis and potential therapies, Arthritis Res. Ther. 9 (2007) S6.
[7] C. Liu, Z. Zhou, K. Li, Improved corrosion resistance of CoCrMo alloy with self-passivation ability facilitated by carbon ion implantation, Electrochim. Acta 241 (2017) 331–340.
[8] J. Lutz, S. Mändl, Reduced tribocorrosion of CoCr alloys in simulated body fluid after nitrogen insertion, Surf. Coat. Technol. 204 (2010) 3043–3046.
[9] S. Valkov, M. Ormanova, P. Petrov, Surface manufacturing of materials by high energy fluxes, in: Mohammad Asaduzzaman Chowdhury (ed.), Advanced Surface Engineering Research, publisher: IntechOpen, 2018, pp. 69–87.
[10] X. Wei, W. Li, B. Liang, B. Li, J. Zhang, L. Zhang, Z. Wang, Surface modification of Co–Cr–Mo implant alloy by laser interference lithography, Tribol. Int. 97 (2016) 212–217.
[11] C. Song, M. Zhang, Y. Yang, D.i. Wang, Y.u. Jia-kuo, Morphology and properties of CoCrMo parts fabricated by selective laser melting, Mater. Sci. Eng. A 713 (2018) 206–213.
[12] C. Zhang, P. Lv, H. Xia, Z. Yang, S. Konovalov, X. Chen, Q. Guan, The microstructure and properties of nanostructured Cr-Al alloying layer fabricated by high-current pulsed electron beam, Vacuum 167 (2019) 263–270.
[13] V. Karansky, A. Klimov, S. Smirnov, Structural transformations in Mn–Zn ferrite under low-energy electron beam treatment, Vacuum 173 (2020), 109115.
[14] D. Wei, X. Wang, R. Wang, H. Cui, Surface modification of 5CrMnMo steel with continuous scanning electron beam process, Vacuum 149 (2018) 118–123.
[15] C. Ramskogler, F. Warchomicka, S. Mostofi, A. Weinberg, C. Sommitsch, Innovative surface modification of Ti6Al4V alloy by electron beam technique for biomedical application, Mater. Sci. Eng. C 78 (2017) 105–113.
[16] M. Ormanova, P. Petrov, D. Kovacheva, Electron beam surface treatment of tool steels, Vacuum 135 (2017) 7–12.
[17] D. Zaguliaev, S. Konovalov, Y. Ivanov, V. Gromov, E. Petrikova, Microstructure and mechanical properties of doped and electron-beam treated surface of hypereutectic Al-11.1%Si alloy, J. Mater. Res. Technol. 8 (5) (2019) 3835–3842.
[18] Y. Ivanov, V. Gromov, D. Zagulyaev, S. Konovalov, A. Semin, Y. Rubannikova, Formation and evolution of structure and phase composition of hypoeutectoid silumin on electron beam processing, J. Surf. Invest. X-ray, Synchrot. Neutron Tech. 13 (5) (2019) 809–813.
[19] H. Cui, R. Wang, D. Wei, J. Huang, J. Guo, X. Li, Surface modification of the carbon tool steel by continuous scanning electron beam process, Nucl. Instrum. Methods Phys. Res. Sect. B 440 (2019) 156–162.
[20] D. Zaguliaev, V. Gromov, Y.u. Rubannikova, S. Konovalov, Y.u. Ivanov, D. Romanov, A. Semin, Structure and phase states modification of AL-11SI-2CU alloy processed by ion-plasma jet and pulsed electron beam, Surf. Coat. Technol. 383 (2020), 125246.
[21] S.-H. Sun, Y. Koizumi, S. Kurosu, Y.-P. Li, A. Chiba, Phase and grain size inhomogeneity and their influences on creep behavior of Co–Cr–Mo alloy additive manufactured by electron beam melting, Acta Mater. 86 (2015) 305–318.
[22] P. Stenlund, S. Kurosu, Y. Koizumi, F. Suska, H. Matsumoto, A. Chiba, A. Palmquist, Osseointegration enhancement by Zr doping of Co-Cr-Mo implants fabricated by electron beam melting, Addit. Manuf. 6 (2015) 6–15.
[23] X.P. Tan, P. Wang, Y. Kok, W.Q. Toh, Z. Sun, S.M.L. Nai, M. Descoins, D. Mangelinck, E. Liu, S.B. Tor, Carbide precipitation characteristics in additive manufacturing of Co-Cr-Mo alloy via selective electron beam melting, Scr. Mater. 143 (2018) 117–121.
[24] S. Valkov, S. Parshorov, A. Andreeva, M. Nikolova, P. Petrov, Surface modification of Co-Cr-Mo alloys by electron-beam treatment, IOP Conf. Series Mater. Sci. Eng. 1056 (2021), 012008.
[25] M.S. Węglowski, S. Błacha, A. Phillips, Electron beam welding – techniques and trends – review, Vacuum 130 (2016) 72–92.
[26] A. Mani, Salinas-Rodriguez, H.F. Lopez, Deformation induced FCC to HCP transformation in a Co–27Cr–5Mo–0.05C alloy, Mater. Sci. Eng. A 528 (2011) 3037–3043.
[27] D. Wei, Y. Koizumi, T. Takashima, M. Nagasako, A. Chiba, Fatigue improvement of electron beam melting-fabricated biomedical Co–Cr–Mo alloy by accessible heat treatment, Mater. Res. Lett. 6 (2018) 93–99.
[28] X.D. Zhang, S.Z. Hao, X.N. Li, C. Dong, T. Grosdidier, Surface modification of pure titanium by pulsed electron beam, Appl. Surf. Sci. 257 (2011) 5899–5902.
[29] T.S.N. Sankara Narayanan, J. Kim, H. Wook Park, High performance corrosion and wear resistant Ti-6Al-4V alloy by the hybrid treatment method, Appl. Surf. Sci. 495 (2019), 144388.
[30] J. Beddoes, M. Bibby, Solidification and casting processes, in: Principles of Metal Manufacturing Processes, Elsevier Ltd., 1999, pp. 18–66, https://doi.org/10.1016/B978-0-340-73162-8.X5000-0.
[31] T. Zhang, P. Li, J. Zhou, C. Wang, X. Meng, S. Huang, Microstructure evolution of laser cladding Inconel 718 assisted hybrid ultrasonic-electromagnetic field, Mater. Lett. 289 (2021), 129401.
[32] Y. Fu, J. Hu, X. Shen, Y. Wang, W. Zhao, Surface hardening of 30CrMnSiA steel using continuous electron beam, Nucl. Instrum. Methods Phys. Res. Sect. B 410 (2017) 207–214.
[33] K.M. Zhang, J.X. Zou, T. Grosdidier, N. Gey, S. Weber, D.Z. Yang, C. Dong, Mechanisms of structural evolutions associated with the high current pulsed electron beam treatment of a NiTi shape memory alloy, J. Vac. Sci. Technol. 25 (1) (2007) 28–36.
[34] J J Hu, G B Zhang, H B Xu, Y F Chen, Microstructure characteristics and properties of 40Cr steel treated by high current pulsed electron beam, Mater. Technol. 27 (4) (2012) 300–303.
[35] J.A. Sandoval-Robles, C.A. Rodríguez, E. García-López, Laser surface texturing and electropolishing of CoCr and Ti6Al4V-ELI alloys for biomedical applications, Materials 13 (22) (2020) 5203.
[36] S. Çelen, H. Özden, Laser-induced novel patterns: As smart strain actuators for new-age dental implant surfaces, Appl. Surf. Sci. 263 (2012) 579–585.
[37] J. Bernard, S. Szmukler-Moncler, S. Pessotto, L. Vazquez, U. Belser, The anchorage of Brånemark and ITI implants of various lengths. I. An experimental study in the canine mandible, Clin. Oral. Implant Res. 14 (2003) 593–600.
[38] P. Lyu, Y. Chen, Z. liu, J. Cai, C. Zhang, Y. Jin, Q. Guan, N. Zhao, Surface modification of CrFeCoNiMo high entropy alloy induced by high-current pulsed electron beam, Appl. Surf. Sci. 504 (2020) 144453.
[39] J. Cai, P. Lv, C.L. Zhang, J. Wu, C. Li, Q.F. Guan, Microstructure and properties of low carbon steel after surface alloying induced by high current pulsed electron beam, Nucl. Instrum. Meth. B 410 (2017) 47–52.
[40] Y. Shen, J. Cai, P. Lv, C.L. Zhang, W. Huang, Q.F. Guan, Microstructures and properties of zirconium-702 irradiated by high current pulsed electron beam, Nucl. Instrum. Meth. B 358 (2015) 151–159.
[41] Z.Q. Zhang, S.Z. Yang, P. Lv, Y. Li, X.T. Wang, X.L. Hou, Q.F. Guan, The microstructures and corrosion properties of polycrystalline copper induced by high-current pulsed electron beam, Appl. Surf. Sci. 294 (2014) 9–14.
[42] J.X. Zou, K.M. Zhang, S.Z. Hao, C. Dong, T. Grosdidier, Mechanisms of hardening, wear and corrosion improvement of 316 L stainless steel by low energy high current pulsed electron beam surface treatment, Thin Solid Films 519 (4) (2010) 1404–1415.
[43] D. Dwivedi, K. Lepkova, T. Becker, Carbon steel corrosion: a review of key surface properties and characterization methods, RSC Adv. 7 (2017) 4580–4610.
[44] M. Liu, D. Qiu, M.-C. Zhao, G. Song, A. Atrens, The effect of crystallographic orientation on the active corrosion of pure magnesium, Scr. Mater. 58 (2008) 421–424.

[45] R. Xin, Y. Luo, A. Zuo, J. Gao, Q. Liu, Texture effect on corrosion behavior of AZ31 Mg alloy in simulated physiological environment, Mater. Lett. 72 (2012) 1–4.
[46] B. Šesták, Modern aspects of plastic deformation in metals, Czech. J. Phys. 22 (1972) 270–285.
[47] T. Mitchell, A. Heuer, Dislocations and Mechanical Properties of Ceramics, In: F.R. N. Nabarro, J.P. Hirth (ed.), Dislocation in solids, publisher: Elsevier Ltd., vol. 12 (2004) pp. 339-402.
[48] S. Valkov, M. Ormanova, P. Petrov, Electron-beam surface treatment of metals and alloys: techniques and trends, Metals 10 (2020) 1219.